

This is the peer reviewed version of the following article: Zhao, R., Zhang, X. X., & Wen, C. Y. (2020). Theoretical modeling of porous coatings with simple microstructures for hypersonic boundary-layer stabilization. *AIAA Journal*, 58(2), 981-986, which has been published in final form at <https://doi.org/10.2514/1.J058403>. © 2019 by the American Institute of Aeronautics and Astronautics, Inc. All rights reserved.

# Theoretical Modeling of Porous Coatings with Simple Microstructures for Hypersonic Boundary-Layer Stabilization

R. Zhao\* and X. X. Zhang<sup>†</sup>

*Beijing Institute of Technology, 100081 Beijing, People's Republic of China*

and

C. Y. Wen<sup>‡</sup>

*The Hong Kong Polytechnic University, Kowloon, Hong Kong, People's Republic of China*

<https://doi.org/10.2514/1.J058403>

## Nomenclature

$A_r$	=	pore aspect ratio, $2b/H$
$b$	=	half-width of square pore, radius of circular pore, m
$c$	=	sound speed, m/s
$H$	=	thickness of porous layer, m
$p$	=	pressure, Pa
$R$	=	reflection coefficient
$t$	=	time, s
$x, y, z$	=	coordinates
$Z$	=	porous layer impedance, $\text{kg}/(\text{m}^2 \cdot \text{s})$
$\rho$	=	density, $\text{kg}/\text{m}^3$
$\phi$	=	porosity

## Subscripts

$h$	=	waves in the pore
$i$	=	incident waves
$r$	=	diffracted waves

## I. Introduction

**H**YPERSONIC cruise vehicles flying at low angles of attack and high lift-to-drag ratios, such as the X-43A, are normally designed with predominantly two-dimensional (2D) shapes and relatively sharp leading edges. When a hypersonic flow passes such a configuration, the acoustic Mack second mode is considered to be the major instability leading to boundary-layer transition from laminar to

turbulent flow, which suggests that the laminar run can be increased by the stabilization of the second mode [1–4]. Among the various techniques that could suppress or attenuate the Mack second mode [5], the use of porous coating has been demonstrated to have a minimal effect on the mean flow but to greatly suppress the Mack second mode [6–10], and it is considered to be one of the most promising control techniques in this context.

In addition to the use of direct numerical simulations of the flow-field within the microstructures to determine the stabilization effect on the hypersonic boundary layer [11–13], the acoustic impedance boundary condition of the vertical velocity at the wall ( $v'_w = p'_w/Z$ ) is usually adopted to model the porous coating. This treatment saves computational resources for numerical simulations [14–20] and assists the linear stability theory (LST) analysis [7,8,21,22]. Here,  $Z$  is the surface impedance, which is a complex quantity that depends on properties of the wall material, porosity parameters, mean flow characteristics on the wall surface, and flow perturbation parameters such as wave frequency and wavelength.  $v'_w$  and  $p'_w$  are the vertical velocity and pressure perturbations, respectively. Fedorov et al. [7] were the first to develop a formulation of  $Z$  for equally spaced cylindrical blind pores by applying the theory of sound wave propagation in thin and long tubes. They subsequently proposed analytical solutions, hereinafter called Fedorov's models, for slits and pores of circular, rectangular, and triangular cross sections, taking account of gas rarefaction effects [23]. Although Fedorov's models have been widely applied to study the stabilization effect of porous coatings, the solutions were derived based on the acoustic characteristics of a single slit or pore and consequently neglect the couplings among adjacent units as well as their contribution to the overall impedance. This simplification is considered to be responsible for the low-frequency shift of the reflection curves [21,24], resulting in a possible frequency mismatch between the most amplified Mack second-mode instability wave and the minimum reflection property of microstructures in the process of optimizing the coating. Recently, Zhao et al. [25] used the plane wave expansion method [26–28] to improve Fedorov's slit model by considering high-order diffracted waves when the acoustic disturbance penetrates the porous surface. In this way, wave scattering and coupling effects are taken into account, with a consequent improvement in the accuracy of predicted reflection frequency. The present note extends the plane wave expansion method to derive impedance models for porous coatings with three-dimensional (3D) pores of circular and square cross sections, which are considered more practical for engineering applications. The accuracy of the predicted reflection frequency is compared with that of Fedorov's models and the effect of pore shape is also discussed.

## II. Theoretical Model

As shown in Fig. 1, the porous coating is taken to be a rigid surface that is periodically corrugated with subwavelength pores of circular or square cross section and is of infinite extension in the  $x$  and  $z$  directions. In accordance with the definitions of the geometrical parameters in previous research [25],  $H$  and  $s$  are the pore depth and unit-cell period, respectively, and  $b$  is the radius in the case of a circular pore and the half-width in the case of a square pore. The aspect ratio is defined as  $Ar = 2b/H$  for both kinds of pores, and the porosity is defined as  $\phi = \pi b^2/s^2$  for a circular pore and  $\phi = 4b^2/s^2$  for a square pore. The coating is assumed to be located in a quiescent atmosphere with uniform and constant density  $\rho$  and sound speed  $c$ .

The acoustic field of an arbitrary incident plane wave penetrating the coating surface can be expressed as (the time dependence  $e^{-j\omega t}$  is omitted for simplicity)

\*Associate Professor, School of Aerospace Engineering; also Research Assistant, Department of Mechanical Engineering; also The Hong Kong Polytechnic University, Kowloon, Hong Kong, People's Republic of China; zr@bit.edu.cn.

<sup>†</sup>Graduate Student, School of Aerospace Engineering.

<sup>‡</sup>Professor, Department of Mechanical Engineering; cywen@polyu.edu.hk (Corresponding Author).

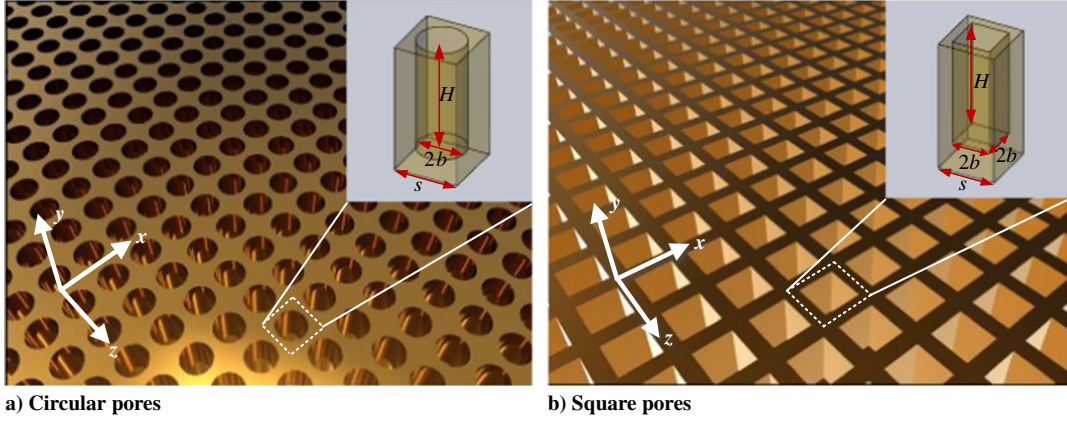


Fig. 1 Schematic illustrations of porous coatings with pores of different cross sections.

$$\begin{aligned}
 p_i &= e^{jk_x x} e^{jk_z z} e^{-jk_y y}, \\
 v_{y,i} &= \frac{1}{j\rho\omega} \frac{\partial p_i}{\partial y} = -\frac{k_y}{\rho\omega} e^{jk_x x} e^{jk_z z} e^{-jk_y y}
 \end{aligned} \quad (1)$$

where  $p_i$  is the incident pressure,  $v_{y,i}$  is the  $y$  component of the particle velocity, and  $j = \sqrt{-1}$ .  $k_x$  and  $k_z$  are the parallel  $x$  and  $z$  momenta, respectively.  $k_y = (k_0^2 - k_x^2 - k_z^2)^{1/2}$  is the perpendicular momentum, in which  $k_0 = \omega/c$  is the wavenumber, with  $\omega$  being the angular frequency. The reflected pressure field  $p_r^{(m,n)}$  and  $y$ -component particle velocity  $v_{y,r}^{(m,n)}$  of the  $(m, n)$ -th-order diffracted wave are expressed as

$$\begin{aligned}
 p_r^{(m,n)} &= R_{mn} e^{jk_x^{(m)} x} e^{jk_z^{(n)} z} e^{jk_y^{(m,n)} y}, \\
 v_{y,r}^{(m,n)} &= \frac{k_y^{(m,n)}}{\rho\omega} R_{mn} e^{jk_x^{(m)} x} e^{jk_z^{(n)} z} e^{jk_y^{(m,n)} y}
 \end{aligned} \quad (2)$$

Here,  $k_x^{(m)} = k_x + (2\pi m/s)$ ,  $k_z^{(n)} = k_z + (2\pi n/s)$ , and  $k_y^{(m,n)} = \sqrt{k_0^2 - (k_x^{(m)})^2 - (k_z^{(n)})^2}$ ,  $m, n \in \mathbf{Z}$ .  $R_{mn}$  is the reflection coefficient of the  $(m, n)$ -th-order diffraction. Inside the pore, the fundamental wave mode dominates in the long-wavelength limit ( $2b \ll \lambda_{acs}$ , where  $\lambda_{acs}$  is the wavelength of the incident acoustic wave), and the sound pressure and particle velocity within the pore are given by

$$\begin{aligned}
 p_h &= C_1 e^{jk_h y} + C_2 e^{-jk_h y}, \\
 v_{y,h} &= \frac{k_h}{\rho\omega} (C_1 e^{jk_h y} - C_2 e^{-jk_h y})
 \end{aligned} \quad (3)$$

Here, the dynamic density  $\tilde{\rho}$ , compressibility  $\tilde{C}$ , and wavenumber  $k_h$  are complex and frequency-dependent quantities owing to the existence of thermal and viscous boundary layers inside the narrow pore:

$$\begin{aligned}
 \tilde{\rho} &= \rho/\Psi_\nu, \quad \tilde{C} = \frac{\gamma - (\gamma - 1)\Psi_t}{\rho c^2}, \\
 k_h^2 &= \omega^2 \tilde{\rho} \tilde{C} = k_0^2 \frac{\gamma - (\gamma - 1)\Psi_t}{\Psi_\nu}
 \end{aligned} \quad (4)$$

in which, for a circular pore,

$$\Psi_{v||t} = -\frac{J_2(bk_{v||t})}{J_0(bk_{v||t})} \quad (5)$$

with  $J_0$  and  $J_2$  being Bessel functions of zeroth and second order, respectively, whereas, for a square pore,

$$\begin{aligned}
 \Psi_{v||t} &= 2k_{v||t}^2 \sum_{M=0}^{\infty} \left( \frac{1}{\alpha_M M'} \right)^2 \left( 1 - \frac{\tan(\alpha_M b)}{\alpha_M b} \right), \\
 \alpha_M &= \sqrt{k_{v||t}^2 - (M'/b)^2}, \quad M' = \left( M + \frac{1}{2} \right) \pi, \quad (M = 0, 1, 2, \dots)
 \end{aligned} \quad (6)$$

In both Eqs. (5) and (6),  $k_{v||t}$  has the same form:

$$k_{v||t}^2 = \begin{cases} k_v^2 = j\omega \frac{\rho}{\mu}, & \text{viscous wave number} \\ k_t^2 = j\omega \frac{\rho C_p}{\kappa}, & \text{thermal wave number} \end{cases} \quad (7)$$

The subscript  $v||t$  is either  $v$  or  $t$ , denoting the effect of the viscous or thermal boundary layer, respectively. In the above equations,  $\kappa$  is the thermal conductivity,  $\mu$  is the viscosity, and  $\gamma = C_p/C_v$  is the ratio of the specific heat at constant pressure  $C_p$  to the specific heat at constant volume  $C_v$ .

The bottom of the cavity is rigid ( $v_{y,h}|_{y=-H} = 0$ ) and thus we have  $C_1 = C_2 e^{2jk_h H} \equiv C e^{2jk_h H}$ . At the interface, the continuity of the sound pressure requires that the mean pressure over the opening area at  $y = 0^+$  equals the pressure inside the pore at  $y = 0^-$ . Application of this condition to the case of a circular pore gives

$$\begin{aligned}
 \frac{1}{\pi b^2} \iint_{x^2+z^2 \leq b^2} \left( e^{jk_x x} e^{jk_z z} + \sum_{m,n=-\infty}^{+\infty} R_{mn} e^{jk_x^{(m)} x} e^{jk_z^{(n)} z} \right) dx dz \\
 = C(1 + e^{2jk_h H})
 \end{aligned} \quad (8)$$

After a simple process of deduction, we have

$$\sum_{m,n=-\infty}^{+\infty} (\delta_{mn,00} + R_{mn}) S_{mn} = C(1 + e^{2jk_h H}) \quad (9)$$

where  $S_{mn} = (1/\pi b^2) \iint_{x^2+z^2 \leq b^2} e^{jk_x^{(m)} x} e^{jk_z^{(n)} z} dx dz = \left( 2J_1 \left( b \sqrt{(k_x^{(m)})^2 + (k_z^{(n)})^2} \right) / b \sqrt{(k_x^{(m)})^2 + (k_z^{(n)})^2} \right)$  is the overlap integral between the  $(m, n)$ -th-order diffracted mode and the fundamental mode inside the circular pore;  $\delta_{mn,00}$  is the Kronecker delta function defined as  $\delta_{mn,00} = 1$  for  $(m, n) = (0, 0)$  and  $\delta_{mn,00} = 0$  otherwise;  $J_1$  is the Bessel function of first order.

The continuity requirement on the particle velocity  $v_y$  is that it should be continuous at the opening area and equal to zero elsewhere:

$$\begin{aligned}
& -\frac{k_y}{\rho\omega} e^{jk_x x} e^{jk_z z} + \sum_{m,n=-\infty}^{+\infty} \frac{k_y^{(m,n)}}{\rho\omega} R_{mn} e^{jk_x^{(m)} x} e^{jk_z^{(n)} z} \\
& = \begin{cases} \frac{k_h}{\tilde{\rho}\omega} C(e^{2jk_h H} - 1) & x, z \in \{x, z | x^2 + z^2 \leq b^2\} \\ 0 & x, z \notin \{x, z | x^2 + z^2 \leq b^2\} \end{cases} \quad (10)
\end{aligned}$$

We multiply the above equation by  $e^{-jk_x^{(r)} x} e^{-jk_z^{(q)} z}$  (where  $r$  and  $q$  are integers) and average over the unit cell area

$$\begin{aligned}
& \frac{1}{s^2} \sum_{m,n=-\infty}^{+\infty} \int_{x,z=-s/2}^{x,z=s/2} \frac{k_y^{(m,n)}}{\rho\omega} (\delta_{mn,00} - R_{mn}) e^{j(k_x^{(m)} - k_x^{(r)})x} e^{j(k_z^{(n)} - k_z^{(q)})z} dx dz \\
& = \frac{1}{s^2} \iint_{x^2+z^2 \leq b^2} \frac{k_h}{\tilde{\rho}\omega} C(1 - e^{2jk_h H}) e^{-jk_x^{(r)} x} e^{-jk_z^{(q)} z} dx dz \quad (11)
\end{aligned}$$

Using the orthogonality of the exponential function, we can solve Eq. (11) to give

$$R_{rq} = \delta_{rq,00} - C(1 - e^{2jk_h H}) \phi \frac{\rho k_h}{\tilde{\rho} k_y^{(r,q)}} S_{rq} \quad (12)$$

Substituting Eq. (12) into the pressure continuity condition (9) yields

$$2S_{00} - C(1 - e^{2jk_h H}) \phi \frac{\rho}{\tilde{\rho}} \sum_{r,q=-\infty}^{+\infty} \frac{k_h}{k_y^{(r,q)}} S_{rq}^2 = C(1 + e^{2jk_h H}) \quad (13)$$

The coefficient  $C$  is then determined as

$$C = \frac{2S_{00}}{(1 + e^{2jk_h H}) + (1 - e^{2jk_h H}) \phi (\rho/\tilde{\rho}) \sum_{r,q=-\infty}^{+\infty} (k_h/k_y^{(r,q)}) S_{rq}^2} \quad (14)$$

and is substituted into Eq. (12). With the relation  $-j \tan(k_h H) = (1 - e^{2jk_h H}/1 + e^{2jk_h H})$ , the reflection coefficients of Eq. (12) can then be expressed as

$$R_{mn} = \delta_{mn,00} + \frac{2j \tan(k_h H) (\rho/\tilde{\rho}) \phi (k_h/k_y^{(m,n)}) S_{mn}}{1 - j \tan(k_h H) (\rho/\tilde{\rho}) \phi \sum_{r,q=-\infty}^{+\infty} (k_h/k_y^{(r,q)}) S_{rq}^2} \quad (15)$$

Assuming normal incidence of the Mack second mode (i.e.,  $k_x = 0$ ,  $k_z = 0$ , and  $k_y = k_0$ ) [24] and that the periodic spacing  $s \ll \lambda_{acs}$ , the effective impedance  $Z$  of the porous coating with circular pores can be derived as

$$\begin{aligned}
Z & = \frac{p}{v} \Big|_{y=0} = \frac{(1/s^2) \int_{x,z=-s/2}^{x,z=s/2} (p_i + \sum_{m,n=-\infty}^{+\infty} p_r^{(m,n)}) dx dz}{(1/s^2) \int_{x,z=-s/2}^{x,z=s/2} (v_{y,i} + \sum_{m,n=-\infty}^{+\infty} v_{y,r}^{(m,n)}) dx dz} \\
& = \rho c \frac{R_{00} + 1}{R_{00} - 1} \quad (16)
\end{aligned}$$

where the reflection coefficient of zeroth-order diffraction (specular refraction) is

$$R_{00} = 1 + \frac{2j \tan(k_h H) (\rho/\tilde{\rho}) \phi (k_h/k_0)}{1 - j \tan(k_h H) (\rho/\tilde{\rho}) \phi \sum_{r,q=-\infty}^{+\infty} (k_h S_{rq}^2 / \sqrt{k_0^2 - (2r\pi/s)^2} - (2q\pi/s)^2)} \quad (17)$$

For the case of a square pore, by applying the continuity requirements of pressure and velocity at the unit surface, a derivation similar to that from Eqs. (8–14) leads to expressions for the impedance and for the reflection coefficients that are similar to those in Eq. (16) and in Eqs. (15) and (17), respectively, except that

$S_{mn} = (1/4b^2) \int_{x,z=-b}^{x,z=b} e^{jk_x^{(m)} x} e^{jk_z^{(n)} z} dx dz = \text{sinc}(k_x^{(m)} b) \text{sinc}(k_z^{(n)} b)$ . Because the derivation includes the higher-order diffracted modes, the mutual wave coupling among neighboring pores is taken into account. In particular, Eq. (17) reduces to Fedorov's model if all higher-order modes are neglected and the porosity  $\phi$  is allowed to tend to zero (so that the local oscillations inside each pore become independent), and reads

$$R_{00} = 1 + \frac{2j \tan(k_h H) (\rho/\tilde{\rho}) \phi (k_h/k_0)}{1 - j \tan(k_h H) (\rho/\tilde{\rho}) \phi (k_h/k_0)} \quad (18)$$

### III. Validation and Discussion

To mimic the operational environment as much as possible, a steady flow calculation of a Mach 6 hypersonic flat-plate flow was first conducted [29]. The freestream flow conditions are referred to the wind tunnel experiment of Bountin et al. [30]: Mach number  $Ma_\infty = 6.0$ , unit Reynolds number  $Re_\infty = 10.5 \times 10^6 \text{ m}^{-1}$ , and temperature  $T_\infty = 43.18 \text{ K}$ . The wall is isothermal with a temperature of  $T_w = 293 \text{ K}$ . The flow parameters at the wall ( $\rho_w = 5.59 \times 10^{-3} \text{ kg/m}^3$  and  $p_w = 470.1 \text{ Pa}$ ) are obtained at 75% of the plate length where the Mack second mode dominates [29,30], and are provided to test the acoustic characteristics of the porous coatings. The following assumptions are also hypothesized: 1) a continuum without rarefaction effect, 2) a perfect gas with Prandtl number  $Pr = 0.72$  and  $\gamma = 1.4$ , and 3) Sutherland-law temperature-dependent viscosity/conductivity [24]. Two corresponding acoustic Reynolds numbers,  $Re_{acs} = \rho_w c_w b / \mu_w$  of 10 and 100, are chosen [24]. The aspect ratio  $Ar$ , porosity  $\phi$ , and the normalized incident-wave frequency ( $f_{acs} = fH/c = H/\lambda_{acs}$ ) are varied in the range of 0.06–0.5, 0.2–0.8, and 0–1.5, respectively. These porous parameters are also relevant for practical applications in high-altitude hypersonic flight [21,24]. Figure 2 compares the reflection coefficient contours obtained from the proposed model and Fedorov's model. It is observed that the results of two models are consistent at lower  $f_{acs}$ , and diverge when  $f_{acs}$  increases for both kinds of coatings (circular and square pores). As addressed in Ref. [25], when  $f_{acs}$  increases, the interactions among adjacent pores become strong and the higher-order terms in the proposed model take effect, yielding the differences from the Fedorov's model. By including the data from a finite element solver (COMSOL Multiphysics), the reflection coefficient distributions at different combinations of  $Ar$ ,  $\phi$ , and  $Re_{acs}$  are compared in Fig. 3. In the previous investigations of the porous coating with 2D slits [21,24,25,31], a resonant mode of  $f_{res} = \phi/Ar$  with  $|R|$  approaching unity was found. For coatings with 3D pores, when  $\lambda_{acs}$  approaches  $s$ , resonant modes can still be found at  $f_{res} = (2/\sqrt{\pi})(\sqrt{\phi}/Ar)$  for circular pores (in particular,  $f_{res} = 1.26$  in Fig. 3c) and at  $f_{res} = \sqrt{\phi}/Ar$  for square pores (in particular,  $f_{res} = 1.12$  in Fig. 3d). The predicted reflection coefficients by the proposed model are in good agreement with the numerical results up to the limit  $\lambda_{acs} = s$ , whereas that by the Fedorov's models tend to be shifted to the higher  $f_{acs}$ . Notably, when the interaction of the scattered waves at the porous surface becomes strong (i.e., when  $f_{acs}$  approaches  $f_{res}$ ), the predictions by Fedorov's model deviate from the numerical results. In addition, a

possible coupling between diagonal pores ( $\lambda_{acs} = \sqrt{2}s$ ) is not found. The acoustic Reynolds number,  $Re_{acs}$ , mainly affects the oscillatory behavior of the reflection coefficient. At lower  $Re_{acs}$  (e.g.,  $Re_{acs} = 10$  in Fig. 2a), the viscosity dissipates the acoustic energy in deep pores (e.g.,  $Ar = 0.2$ ) without additional reflection from the

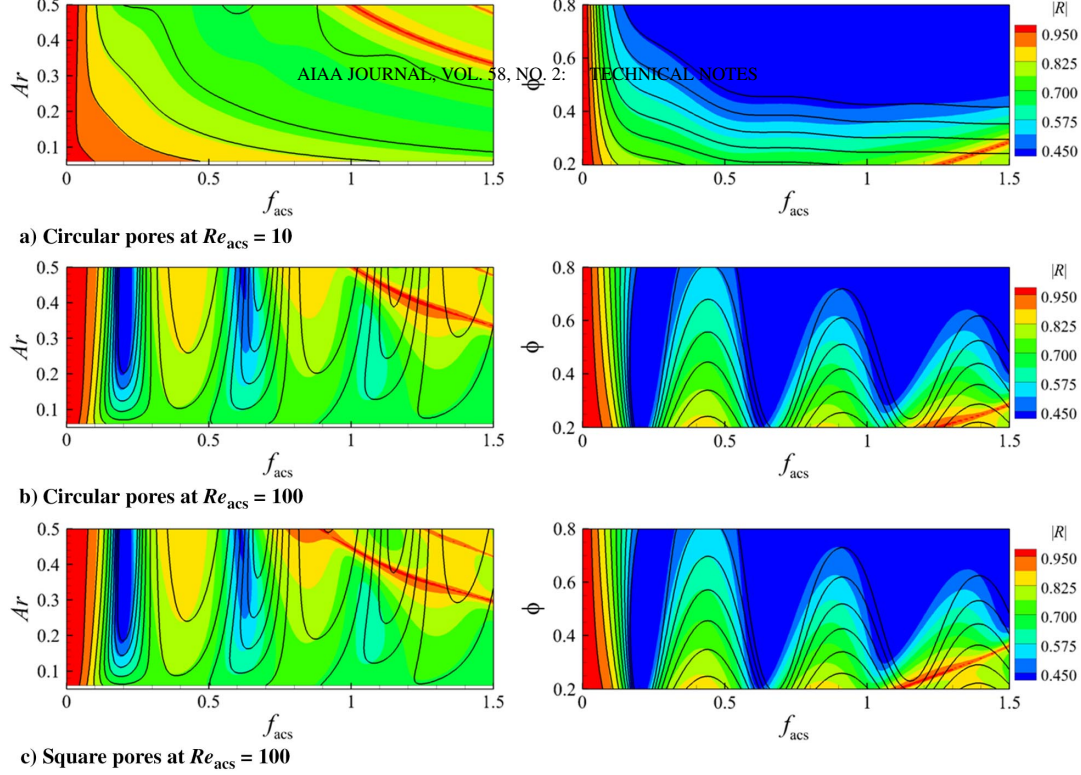


**Fig. 2** Reflection coefficient contours from the proposed model (color contours) and Fedorov's model (black solid lines). Left column:  $\phi$  is kept constant and  $\phi = 0.2$ . Right column:  $Ar$  is kept constant and  $Ar = 0.4$ .

pore bottoms, and the reflection coefficient monotonically decreases with frequency in Fig. 3a. At higher  $Re_{acs}$  (e.g.,  $Re_{acs} = 100$  in Figs. 2b and 2c), reflections from the pore bottoms lead to destructive/constructive reinforcement at some specific frequencies [24], causing the resonant-like curves in Figs. 3b–3d.

Notably, Sousa et al. [19] have made comparisons of measured and predicted absorption coefficients, using the inverse Helmholtz solver, the homogeneous absorber theory, and the model for acoustic impedance of a porous surface with random porosity used by Fedorov et al. [8] for the classical  $C/C$  under different base pressures. The

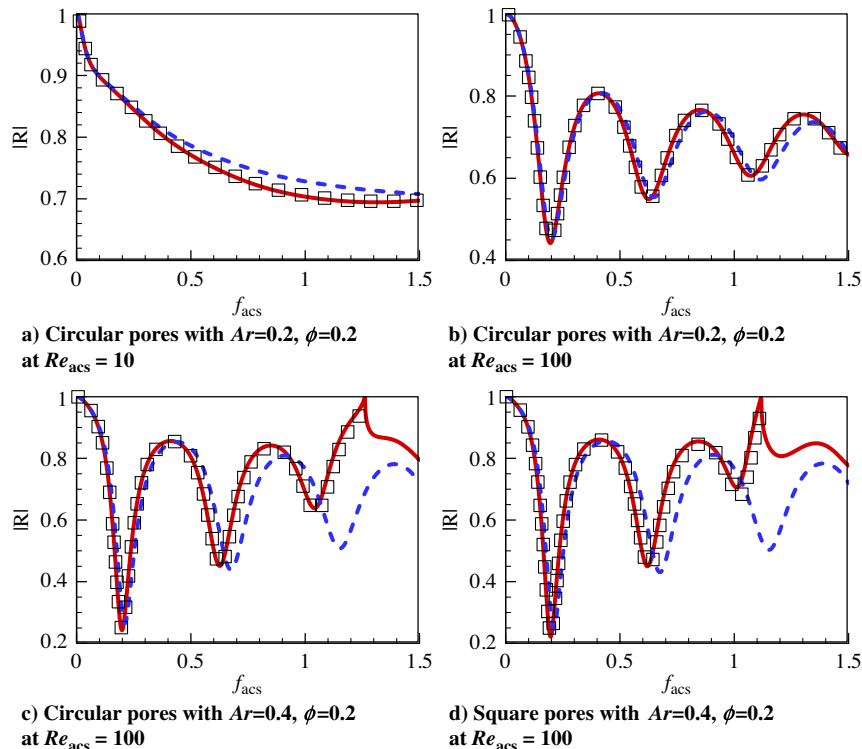


**Fig. 3** Comparison of reflection coefficient amplitude from COMSOL (black square), the proposed model (red solid curve), and Fedorov's model (blue dashed curve).

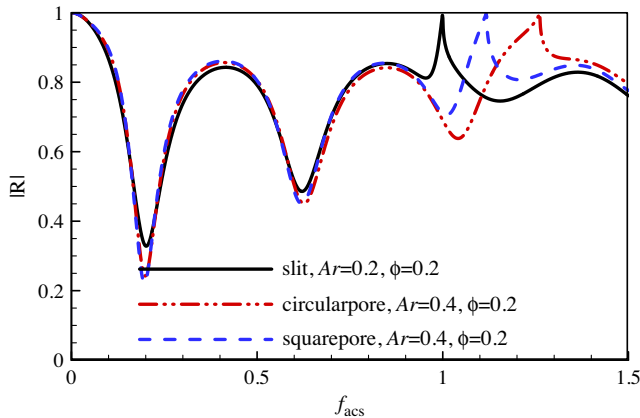


**Fig. 4** Comparison of the reflection coefficient amplitude distributions for slits or pores with the same hydraulic diameter.

discrepancies between the measured and predicted absorption coefficients may be partially attributed to the lack of considering of the scattering effect in the models. More in-depth investigations of the scattering effects on the  $C/C$  composite with an irregular porous surface will be conducted in the future.

According to previous research [11], the stabilization effects of coatings with different slit or pore shapes could be collapsed in good agreement for the same hydraulic diameter  $d_h = 4A_p/C$ , where  $A_p$  is the slit or pore area and  $C$  is the circumference. In line with this, and for the same values of  $\phi$  and  $H$ , the predicted reflection coefficients are generally consistent with each other up to the resonant frequency of the slits (Fig. 4).

#### IV. Conclusions

In the present Note, the theoretical impedance models have been developed to describe the acoustic characteristics of plane ultrasonic acoustic waves impinging on porous coatings corrugated with sub-wavelength pores of circular or square cross section. The proposed models consider high-order diffracted modes and therefore incorporate scattered-wave interactions among adjacent pores. In contrast with the results of Fedorov's models, the predicted reflection coefficients have been shown to be consistent with numerical results from a finite element solver (COMSOL Multiphysics), and the coupling modes induced by neighboring pores are reproduced well. The distributions of the reflection coefficient show the oscillatory behavior at higher acoustic Reynolds numbers; otherwise they monotonically decrease especially for deep pores. Additionally, the acoustic characteristics are in general agreement for coatings with different slit or pore shapes, provided that these have the same hydraulic diameter  $d_h$ , porosity  $\phi$ , and depth  $H$ . In a future study, the stabilization effect on the Mack second mode will be investigated by spatially resolving the flowfields in the slits or pores in the hypersonic flow using direct numerical simulation. This will allow an evaluation of the accuracy of the proposed impedance models when these are used to provide an acoustic impedance boundary condition at the wall.

#### Acknowledgments

This study was supported by the National Natural Science Foundation of China under Grant Nos. 11872116 and 11774297 and by the Research Grants Council, Hong Kong, under Contract Nos. C5010-14E, 152041/18E, and 152119/18E.

#### References

- [1] Fedorov, A. V., "Temporal Stability of Hypersonic Boundary Layer on Porous Wall: Comparison of Theory with DNS," AIAA Paper 2010-1242, Jan. 2010.
- [2] Fedorov, A. V., "Transition and Stability of High-Speed Boundary Layers," *Annual Review of Fluid Mechanics*, Vol. 43, No. 1, 2011, pp. 79–95.  
<https://doi.org/10.1146/annurev-fluid-122109-160750>

- [3] Malik, M. R., "Prediction and Control of Transition in Supersonic and Hypersonic Boundary Layers," *AIAA Journal*, Vol. 27, No. 11, 1989, pp. 1487–1493.  
<https://doi.org/10.2514/3.10292>
- [4] Zhong, X., and Wang, X., "Direct Numerical Simulation on the Receptivity, Instability, and Transition of Hypersonic Boundary Layers," *Annual Review of Fluid Mechanics*, Vol. 44, No. 1, 2012, pp. 527–561.  
<https://doi.org/10.1146/annurev-fluid-120710-101208>
- [5] Fedorov, A. V., "Prediction and Control of Laminar-Turbulent Transition in High-Speed Boundary-Layer Flows," *Procedia IUTAM*, Vol. 14, 2015, pp. 3–14.  
<https://doi.org/10.1016/j.piutam.2015.03.017>
- [6] Rasheed, A., Hornung, H. G., Fedorov, A. V., and Malmuth, N. D., "Experiments on Passive Hypervelocity Boundary Layer Control Using an Ultrasonically Absorptive Surface," *AIAA Journal*, Vol. 40, No. 3, 2002, pp. 481–489.  
<https://doi.org/10.2514/2.1671>
- [7] Fedorov, A. V., Malmuth, N. D., Rasheed, A., and Hornung, H. G., "Stabilization of Hypersonic Boundary Layers by Porous Coatings," *AIAA Journal*, Vol. 39, No. 4, 2001, pp. 605–610.  
<https://doi.org/10.2514/2.1382>
- [8] Fedorov, A. V., Shpiyuk, A. N., Maslov, A. A., Burov, E. V., and Malmuth, N. D., "Stabilization of a Hypersonic Boundary Layer Using Ultrasonically Absorptive Coating," *Journal of Fluid Mechanics*, Vol. 479, March 2003, pp. 99–124.  
<https://doi.org/10.1017/S0022112002003440>
- [9] Lukashovich, S. V., Morozov, S. O., and Shpiyuk, A. N., "Experimental Study of the Effect of a Passive Porous Coating on Disturbances in a Hypersonic Boundary Layer 1: Effect of the Porous Coating Length," *Journal of Applied Mechanics and Technical Physics*, Vol. 54, No. 4, 2013, pp. 572–577.  
<https://doi.org/10.1134/S002189441304007X>
- [10] Lukashovich, S. V., Morozov, S. O., and Shpiyuk, A. N., "Experimental Study of the Effect of a Passive Porous Coating on Disturbances in a Hypersonic Boundary Layer 2: Effect of the Porous Coating Location," *Journal of Applied Mechanics and Technical Physics*, Vol. 57, No. 5, 2016, pp. 873–878.  
<https://doi.org/10.1134/S002189441605014X>
- [11] Sandham, N. D., and Lüdeke, H., "A Numerical Study of Mach 6 Boundary-Layer Stabilization by Means of a Porous Surface," *AIAA Journal*, Vol. 47, No. 9, 2009, pp. 2243–2252.  
<https://doi.org/10.2514/1.43388>
- [12] Wartemann, V., Lüdeke, H., and Sandham, N. D., "Numerical Investigation of Hypersonic Boundary-Layer Stabilization by Porous Surfaces," *AIAA Journal*, Vol. 50, No. 6, 2012, pp. 1281–1290.  
<https://doi.org/10.2514/1.J051355>
- [13] Kirilovskiy, S. V., Poplavskaya, T. V., Tsyryulnikov, I. S., and Maslov, A. A., "Evolution of Disturbances in the Shock Layer on a Flat Plate in the Flow of a Mixture of Vibrationally Excited Gases," *Thermophysics and Aeromechanics*, Vol. 24, No. 3, 2017, pp. 421–430.  
<https://doi.org/10.1134/S0869864317030106>
- [14] Egorov, I., Fedorov, A., Novikov, A., and Soudakov, V., "Direct Numerical Simulation of Supersonic Boundary-Layer Stabilization by Porous Coatings," AIAA Paper 2007-948, Jan. 2007.
- [15] Wang, X., and Zhong, X., "The Stabilization of a Hypersonic Boundary Layer Using Local Sections of Porous Coating," *Physics of Fluids*, Vol. 24, No. 3, 2012, Paper 034105.  
<https://doi.org/10.1063/1.3694808>
- [16] Lukashovich, S. V., Maslov, A. A., Shpiyuk, A. N., Fedorov, A. V., and Soudakov, V. G., "Stabilization of High-Speed Boundary Layer Using Porous Coatings of Various Thicknesses," *AIAA Journal*, Vol. 50, No. 9, 2012, pp. 1897–1904.  
<https://doi.org/10.2514/1.J051377>
- [17] Wang, X., "Stabilization of a Hypersonic Boundary Layer Using Regular Porous Coating," AIAA Paper 2018-2088, Jan. 2018.
- [18] Sousa, V. C. B., Patel, D. I., Chapelier, J.-B., Wagner, A., and Scalco, C., "Numerical Investigation of Second Mode Attenuation over Carbon/Carbon Surfaces on a Sharp Slender Cone," AIAA Paper 2018-0350, Jan. 2018.
- [19] Sousa, V. C. B., Patel, D., Chapelier, J.-B., Wartemann, V., Wagner, A., and Scalco, C., "Numerical Investigation of Second-Mode Attenuation over Carbon/Carbon Porous Surfaces," *Journal of Spacecraft and Rockets*, Vol. 56, No. 2, 2019, pp. 319–332.  
<https://doi.org/10.2514/1.A34294>
- [20] Scalco, C., Sousa, V. C. B., and Bose, R., "Numerical Investigation of Hypersonic Turbulence Transition Control via Complex Wall Impedance," AIAA Paper 2019-2151, Jan. 2019.
- [21] Brès, G. A., Inkmann, M., Colonius, T., and Fedorov, A. V., "Second-Mode Attenuation and Cancellation by Porous Coatings in a High-Speed

- Boundary Layer,” *Journal of Fluid Mechanics*, Vol. 726, July 2013, pp. 312–337.  
<https://doi.org/10.1017/jfm.2013.206>
- [22] Lv, P., Yu, C., Zhang, Y., and Gong, J., “Numerical Investigation of Ultrasonically Absorptive Coating for Hypersonic Laminar Flow Control,” AIAA Paper 2017-2311, March 2017.
- [23] Kozlov, V. F., Fedorov, A. V., and Malmuth, N. D., “Acoustic Properties of Rarefied Gases inside Pores of Simple Geometries,” *Journal of the Acoustical Society of America*, Vol. 117, No. 6, 2005, pp. 3402–3411.  
<https://doi.org/10.1121/1.1893428>
- [24] Brès, G. A., Colonius, T., and Fedorov, A. V., “Acoustic Properties of Porous Coatings for Hypersonic Boundary-Layer Control,” *AIAA Journal*, Vol. 48, No. 2, 2010, pp. 267–274.  
<https://doi.org/10.2514/1.40811>
- [25] Zhao, R., Liu, T., Wen, C. Y., Zhu, J., and Cheng, L., “Theoretical Modeling and Optimization of Porous Coating for Hypersonic Laminar Flow Control,” *AIAA Journal*, Vol. 56, No. 8, 2018, pp. 2942–2946.  
<https://doi.org/10.2514/1.J057272>
- [26] Wu, T., Cox, T. J., and Lam, Y. W., “From a Profiled Diffuser to an Optimized Absorber,” *Journal of the Acoustical Society of America*, Vol. 108, No. 2, 2000, pp. 643–650.  
<https://doi.org/10.1121/1.429596>
- [27] Schwan, L., Geslain, A., Romero-García, V., and Groby, J. P., “Complex Dispersion Relation of Surface Acoustic Waves at a Lossy Metasurface,” *Applied Physics Letters*, Vol. 110, No. 5, 2017, Paper 051902.  
<https://doi.org/10.1063/1.4975120>
- [28] Liu, T., Liang, S., Chen, F., and Zhu, J., “Inherent Losses Induced Absorptive Acoustic Rainbow Trapping with a Gradient Metasurface,” *Journal of Applied Physics*, Vol. 123, No. 9, 2018, Paper 091702.  
<https://doi.org/10.1063/1.4997631>
- [29] Zhao, R., Wen, C. Y., Tian, X. D., Long, T. H., and Yuan, W., “Numerical Simulation of Local Wall Heating and Cooling Effect on the Stability of a Hypersonic Boundary Layer,” *International Journal of Heat and Mass Transfer*, Vol. 121, June 2018, pp. 986–998.  
<https://doi.org/10.1016/j.ijheatmasstransfer.2018.01.054>
- [30] Bountin, D., Chimitov, T., Maslov, A., Novikov, A., Egorov, I., Fedorov, A., and Utyuzhnikov, S., “Stabilization of a Hypersonic Boundary Layer Using a Wavy Surface,” *AIAA Journal*, Vol. 51, No. 5, 2013, pp. 1203–1210.  
<https://doi.org/10.2514/1.J052044>
- [31] Brès, G. A., Colonius, T., and Fedorov, A. V., “Interaction of Acoustic Disturbances with Micro-Cavities for Ultrasonic Absorptive Coatings,” AIAA Paper 2008-3903, June 2008.